CIRP Annals - Manufacturing Technology 58 (2009) 255–258

Contents lists available at ScienceDirect

CIRP Annals - Manufacturing Technology

journal homepage: http://ees.elsevier.com/cirp/default.asp

Modelling of the Mannesmann effect

A. Ghiotti [a], S. Fanini [a], S. Bruschi (2)[b,*], P.F. Bariani (1)[a]

[a] DIMEG, University of Padova, Via Venezia 1, 35131, Padova, Italy
[b] DIMS, University of Trento, Via Mesiano 77, 38050 Trento, Italy

ARTICLE INFO

Keywords:
Damage
Modelling
Tube piercing

ABSTRACT

The paper presents a new model of the Mannesmann effect. The model is based on a novel damage law that takes into account the effects of pre-existing defects in the working material. Thanks to this feature, the model is capable of making accurate predictions of the location where the fracture will appear under the action of external loading as well as of the time it takes to be generated. An application of the model to a rotary tube piercing operation carried out at elevated temperature is presented and commented.

1. Introduction

The Mannesmann effect (hereafter indicated as ME) refers to the formation of a cavity along the longitudinal axis in bars subjected to radial compression in metalworking operations. Cavities form due to secondary tensile stresses that are induced at the centre of the bar by a highly inhomogeneous deformation in the bar cross-section. The ME can appear under both cold and hot deformation conditions, and it is one of the most serious limitations in processes such as transverse rolling, cogging and rotary swaging of round bars. Unlike these processes, the continuous formation of an axial cavity due to the cycling radial compression action exerted by rotating rolls (Fig. 1) is the principle underlying rotary tube piercing, the most common process to make long, thick-walled seamless pipes, also known as Mannesmann process. The axes of the rolls are skewed in order to pull the bar and force it to advance in the rolling mill. The stationary plug placed at a fixed distance from the location where the cavity develops helps to expand the hole and size the inner tube diameter.

The ME has been extensively investigated using different approaches and models. Depending on the approach, the models can be classified into two groups: *explanatory* models and *predictive* models. The former simply offers an explanation of the cavity development and its location by providing information on the stress state and the velocity field in the material. These models are based on the slip line field theory or upper bound techniques [1] and, more recently, on FE simulations of the deformation process [2–4]. *Predictive* models, on the other hand, are founded on energy-based damage theories [5,6] and provide a more comprehensive description of the process-related causes and phenomena of the ME [7,8]. They can be particularly useful in predicting the process conditions that cause the fracture to occur and propagate. However, according to the damage theories on which they are based, these models prove to be reliable only if the material is free from pre-existing defects. This assumption represents a significant limitation to their application, especially for processes that are carried out at elevated temperatures, where the working material has micro-porosities that have not been eliminated by primary-working operations or is a cast bar—as is common for cogging and rotary tube piercing—with shrinkage cavities in the central zone caused by the solidification pattern. The distribution of the pre-existing defects has a significant influence on the time the defect takes to grow to the critical size and then to generate a fracture. In rotary tube piercing, the distribution of shrinkage cavities in the cross-section of the bar has a significant influence on the value of the distance between the apex of the plug to be maintained during the process and the location on the bar axis where the fracture occurs. With a wider span, the plug meets the cavity zone too late, when the fracture has already propagated and the inner tube wall may get oxidized. With a narrower span, the plug meets the material too early, before the fracture forms, with consequent high wear rate on the plug surface.

In this paper, a new model of the ME is presented, which is capable of accurately predicting: (i) the location where the fracture appears under the action of external loading and (ii) the time it takes to be generated. The model makes use of a novel damage law, which is proposed by the Authors as a modification of the Lemaitre damage law [9,10], taking into account the effects of pre-existing defects in the working material. With this feature, the model presented in the paper overcomes the main limitations of the above-cited models.

The paper is organized into three parts. In the first part (Sections 2 and 3), the general architecture of the model and the industrial application case are presented. In the second part (Sections 4–6), the paper focuses on the three main elements of the model: the material database generation, the FE analysis of the process and the new damage law. Finally, in Section 7, the results from the application of the model to an industrial case are presented and compared to the experimental results from industrial trials.

* Corresponding author.

0007-8506/$ – see front matter © 2009 CIRP.
doi:10.1016/j.cirp.2009.03.099

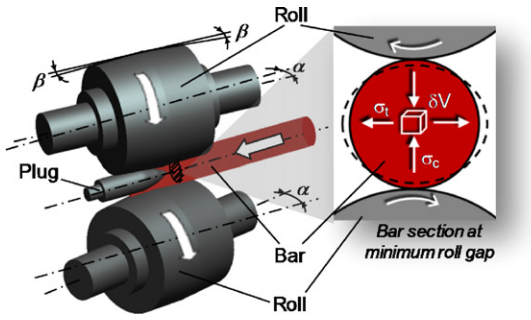

Fig. 1. Sketch of the rotary tube piercing process and secondary tensile stresses in the bar centre.

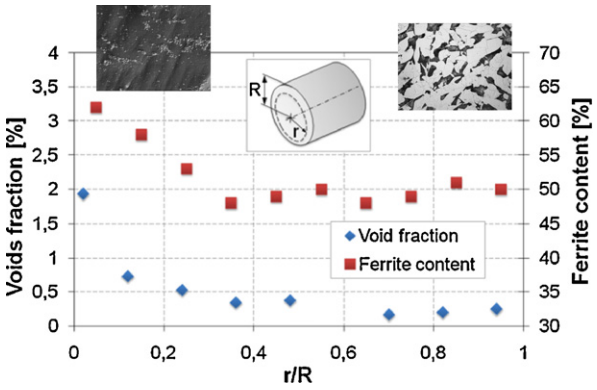

Fig. 2. Void fraction and ferrite content distribution in the bar cross-section.

2. Model architecture

The major requirement that the proposed model has to meet is to predict the location where the fracture appears under the action of external loading and the time it takes to be generated.

According to this requirement, in its implementation and application phases, the model requires the joint use of complementary techniques, both numerical and experimental, organized in three functional modules that are devoted respectively to: (i) generation of the material database, (ii) FE thermo-mechanical analysis of the deformation process, and (iii) calculation of damage evolution.

The material data generated by the first functional module regard microstructure and distribution of the pre-existing defects, and the material rheology and workability. These data are then used for both the FE analysis and the damage calculations.

The main task of the FE analysis carried out by the second functional module is to provide an accurate evaluation of the thermal and mechanical parameters in the material zone where cavities develop. The proposed damage law is implemented in the FE model.

The third functional module provides the evaluation of the continuous evolution of the damage as function of the pre-existing damage, which is provided by the first module, and the process parameters, which are calculated by the FE analysis carried out in the second module.

Details on the experimental and numerical techniques and procedures used in the three modules and the relevant data and results are given in Sections 4–6, with reference to the rotary tube piercing process presented as an application case in Section 3.

3. Application case

The application case refers to a rotary tube piercing process carried out on a Mannesmann rolling mill equipped with a piercing plug, two skew conical rolls and two shoes to support and guide the incoming bar. For the two conical rolls the maximum diameter is 720 mm, their enter and exit angles β are 2.5° and the skew angle α is 6° (see Fig. 1). The workpiece is a 200 mm diameter continuously cast bar made of low-alloyed steel DIN St52 that enters the rolling area at a temperature of 1250 °C. The maximum outer-diameter reduction is equal to 10%, which corresponds to a minimum distance between the rolls of 180 mm. The roll speed is 300 rpm, which corresponds to an axial feeding rate of the bar equal to 380 mm/s.

4. Material data generation

In this section, the testing procedures used in the first functional module are presented together with the relevant data generated for the material of the application case.

4.1. Microstructural analysis and data

Microstructural analysis was carried out on the cross-section of the cast bar to investigate the distribution of the initial void fraction (due to shrinkage) and the ferrite content. To this aim, several samples were cut from bar cross-sections at different distances from the axis. The void fraction and the ferrite content were determined respectively through high contrast image digitalization and light microscopy observations of samples after metallographic preparation. Fig. 2 shows the two similar distributions measured from the axis to the surface of the bar for the void fraction and the ferrite content. According to these measurements, a 60 mm diameter cylindrical core can be identified in the cross-section of the cast bar where the two distributions present a high gradient. Out of this core, the ferrite content is practically constant and the void fraction negligible.

The voids fraction distribution in the core diameter is used to evaluate the initial damage distribution in the third functional module, which is devoted to the calculation of damage evolution (see Section 6).

4.2. Rheological tests and data

The rheological tests generate the true stress–true strain curves of the bar material. These curves are then implemented through a rheological law in the FE model of the process (see Section 5) in order to provide accurate predictions of the thermal and mechanical parameters in the piercing operation, especially in the material zone where cavities develop. With this aim, hot compression tests were carried out on a Gleeble™ 3800 machine with uniform temperatures ranging from 1050 to 1250 °C and constant strain rates from 0.05 to 20 s^{-1}, these being representatives of the operating conditions of the application case. The Hansel–Spittel law was used to represent the dependency of the material flow stress on strain, strain rate and temperature, according to Eq. (1):

$$\bar{\sigma} = 9400.1 \exp(-0.0042T)\bar{\varepsilon}^{0.0125}\dot{\bar{\varepsilon}}^{0.1262} \exp\left(-\frac{0.2079}{\bar{\varepsilon}}\right) [\text{MPa}] \quad (1)$$

4.3. Workability tests and data

The workability tests are used to identify the material constants in the damage law described in Section 6. The tests are uniaxial hot tensile tests on samples cut from different locations in the cross-section of the bar, both inside and outside the core area identified through the microstructural analysis described in Section 4.1 (see scheme in Fig. 3). The tests were carried out on the Gleeble™ 3800 machine, with the temperature and the strain rate kept constant during the tests. The temperature was fixed at 1250 °C for all the tests, while the strain rate ranged from 5×10^{-4} to 0.5 s^{-1} in agreement with the results of preliminary FE simulations of the application case.

As shown in Fig. 3, the sample location has a significant influence on both the material strength and strain at fracture. For the samples cut from the core area, the higher values of void

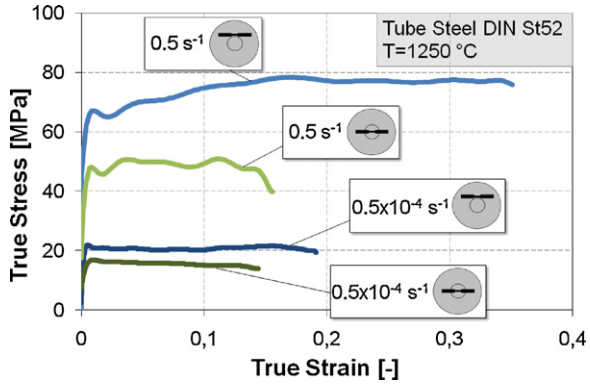

Fig. 3. Material strength vs. strain for samples cut from the centre and periphery of the bar cross-section.

fraction and ferrite amount cause a significant decrease in the material flow strength and the strain at fracture as well.

5. Finite element analysis

The numerical simulations of the thermo-mechanical events occurring inside the cast bar during the piercing operation are provided by a three-dimensional FE model of the process chosen as an application case, which is based on the implicit commercial code Forge® 2007.

The two conical rolls and shoes for the bar alignment were modelled as rigid bodies; an elastic-viscoplastic behaviour was assumed for the bar material according to the Hansel–Spittel law (Eq. (1)). Due to the restricted extension of the contact surfaces, friction and heat transfer at the interfaces between the rolls and bar and between the plug and bar do not have a significant effect on the stress state in the area of damage development and fracture propagation, as confirmed by preliminary sensitivity analyses. A Tresca factor equal to 0.8 was used for the two interfaces, which allows the calculated axial feed of the bar to be very close to the measured value. A constant heat transfer coefficient (HTC) of 10,000 W/(m^2 K) was assumed for the contact at all interfaces and an HTC of 10 W/(m^2 K) was assumed with the environment.

To enhance the accuracy of simulation, very fine meshing parameters were used in the bar central area. To reproduce the fracture propagation, the 'killing element' technique was used, which deletes the elements when the critical damage value is reached.

6. Calculation of damage evolution

In this section, the novel damage law proposed by the Authors is presented. The law takes into account the effects of pre-existing defects in the working material.

6.1. Proposed damage law

The proposed damage law is a modification of the standard Lemaitre law [9,10], based on Continuum Damage Mechanics. According to the novel law, the damage rate $\dot{D}$ is given by Eq. (2).

$$\dot{D} = \left(-\frac{h_c y}{S_0}\right)^{s_1 - s_2 D_{in}} \dot{\bar{\varepsilon}}_p \tag{2}$$

where $\dot{\bar{\varepsilon}}_p$ is the accumulated plastic strain rate; s_1, s_2 and the damage strength S_0 are material constants to be evaluated through inverse analysis applied to the tensile tests described in Section 6.2; h_c is a factor taking into account the effect of compressive stress state on damage evolution and is set equal to 1 in case of tensile stress state, and equal to 0.2 in case of compressive stress state; y and D_{in} are the damage strain energy release rate and the initial damage, respectively, and are defined by Eqs. (3) and (4).

$$-y = \frac{\bar{\sigma}^2}{2E(1-D)^2}\left[\frac{2}{3}(1+\nu) + 3(1-2\nu)\left(\frac{\sigma_H}{\bar{\sigma}}\right)^2\right] \tag{3}$$

$$D_{in} = ae^{-b(r/R)} \tag{4}$$

In Eq. (3), D is the damage variable, E the Young's modulus, ν the Poisson's coefficient, $\bar{\sigma}$ the equivalent stress and $\sigma_H/\bar{\sigma}$ is the stress triaxiality factor.

In Eq. (4), the constant a represents the initial value of the damage D_{in} on the axis of the bar, r is the radius ranging from 0 to the bar radius R. The value of a is calculated through inverse analysis (see Section 6.2). The coefficient b is calculated by the condition $D_{in} = 0$ when r equals the radius of the core area determined through the void distribution analysis.

The damage variable D evolves according to Eq. (2) and the fracture appears when the level of critical damage D_c in Eq. (3) is reached. D_c is calculated through inverse analysis as reported in Section 6.2.

6.2. Constants identification

Inverse analysis is used to determine the five damage constants in Eqs. (2)–(4). They are s_1, s_2, S_0, D_c and a. Their values are identified through a fully automatic procedure as those, which minimise the difference between the force and displacement curves measured in the tensile tests (described in Section 4.3) and the same curves calculated from FE simulations of the tests carried out by using Forge® 2007, where Eqs. (2)–(4) have been implemented. The inverse analysis is applied separately for the identification of the three constants S_0, s_1 and D_c and for the two constants a and s_2. To identify S_0, s_1 and D_c, the data used in the inverse analysis are derived from the tensile tests carried out on the samples cut from the material out of the core area, where the initial damage D_{in} is negligible. Once these three constants related to the non-damaged material are determined and implemented in Eqs. (2) and (3), a and s_2 are identified by inverse analysis from the tensile data of the material in the bar core area. Fig. 4 shows the good agreement between the force and displacement curves measured and obtained at the end of the automatic iterative procedure of the inverse analysis.

The values identified for the five material damage constants are given in Table 1.

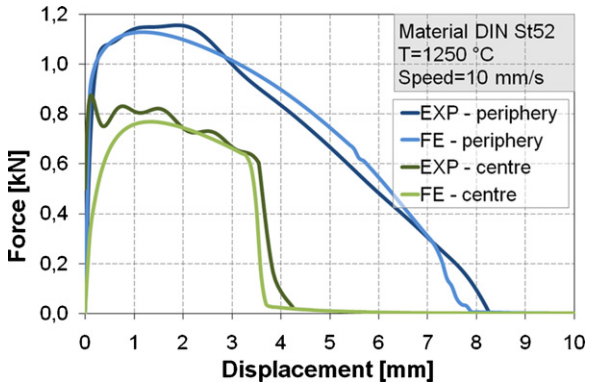

Fig. 4. Numerical inverse analysis fitting in the centre and periphery of the bar cross-section.

Table 1
Damage constants.

s_1	s_2	S_0	D_c	a	b
0.3985	1.5	1.2198	0.58	0.2	17.661

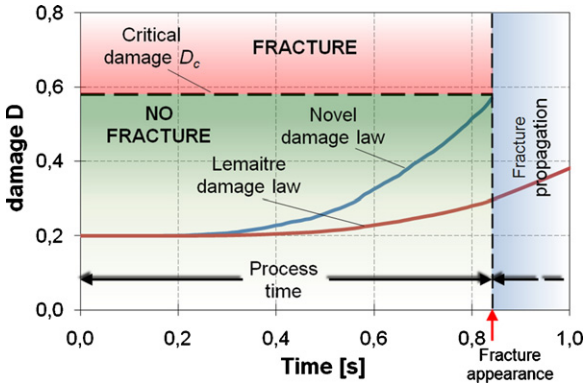

Fig. 5. Damage vs. time as predicted by the Lemaitre standard law (red line) and the proposed law (blue line). (For interpretation of the references to color in this figure legend, the reader is referred to the web version of the article.)

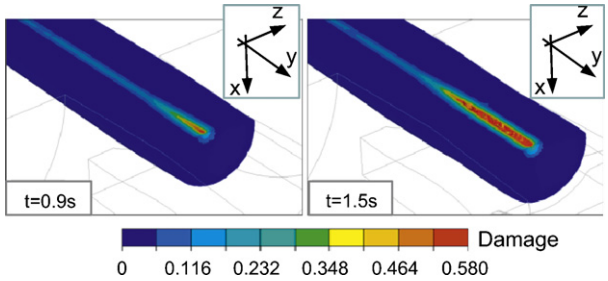

Fig. 6. Localization of the damaged area at the centre of the bar as predicted by the proposed model.

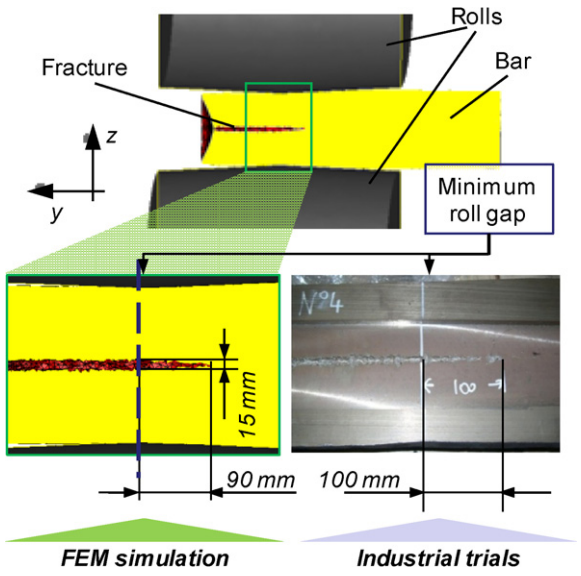

Fig. 7. Fracture length and width from the numerical simulation (left) and experimental measurements (right).

7. Model validation

The model validation was performed by comparing the results of the model predictions with the measurements carried out during experiments on the industrial rolling mill described in Section 3. The comparison was made with reference to: (i) the time the pre-existing damage D_{in} takes to reach the critical value D_c, (ii) the location of the damaged area on the bar cross-section, and (iii) the axial length and radial width of the cavity area caused by fracture propagation. To focus the validation on the ME, both the numerical simulations and the experiments were carried out without the plug.

Fig. 5 shows a comparison of the damage evolution as predicted by standard Lemaitre damage law and by the proposed law. According to the proposed law, the damage takes 0.85 s to reach the critical value D_c, very close to the time of 0.90 s that was measured in the industrial trials through quick stops of the rolling mill. The same time calculated by the standard law results significantly longer.

The predictions of the proposed model proved to be accurate as regards the location of the damaged area as well. Fig. 6 shows the evolution of the damaged area calculated at two different process times. The damage is restricted to the central part of the rod, as confirmed by the experimental observations. Using energy-based damage laws, the damaged areas appear also close to the external surface of the bar.

In Fig. 7, the predictions and measurements of the axial length and radial width of the cavity area after a process time of 1.5 s are compared. According to the industrial practice, the fracture length was measured along the bar axis from the minimum-gap cross-section. From results in Fig. 7, the predictions of the proposed model prove to be accurate, the gap between predictions and measurements being less than 10%.

8. Conclusions

A new model of the ME that makes use of a novel damage law that takes into account the effects of pre-existing defects in the working material was developed. The model proved to be capable of accurate predictions of: (i) the location where the fracture will appear under the action of external loading and (ii) the time it takes to be generated.

The model can be considered general enough to be applied to any process where the Mannesmann effect can appear. It is worth to remark that the model has precise requirements in terms of experimental data and microstructural analysis. In particular, void fraction has to be estimated for each batch produced by continuous casting, in order to determine the initial damage distribution in the bar. The use of statistical methods can reduce the impact of this issue on the industrial suitability of the presented approach, even if the involvement of time-consuming testing could limit the applicability of the model only to large batches.

References

[1] Alexander JM, Brewer RC (1963) *Manufacturing Properties of Materials*. D. van Nostrand.
[2] Gelin JC (1988) Kinematic and Thermal Analysis of Hot Piercing Rolling of Seamless Tubes. *Annals of the CIRP* 37(1):255–258.
[3] Mori K, Osakada K (1990) Finite Element Simulation of Three-dimensional Deformation in Shape Rolling. *International Journal of Numerical Methods in Engineering* 30(8):431–1440.
[4] Komori K (2005) Simulation of Mannesmann Piercing Process by the Three-dimensional Rigid-plastic Finite-element Method. *International Journal of Mechanical Sciences* 47:1838–1853.
[5] Osakada K, Mori K, Hudo H (1978) Prediction of Ductile Fracture in Cold Forging. *CIRP Annals* 27(1):135–138.
[6] Gelin JC (1986) Application of Thermo-viscoplastic Model to the Analysis of Defects in Warm Forming Conditions. *CIRP Annals* 35(1):157–160.
[7] Fanini S, Bruschi S, Ghiotti A (2007) Evaluation of Fracture Initiation in the Mannesmann Piercing Process. *Proceedings of the 10th ESAFORM Conference on Material Forming*, Zaragoza, Spain, 709–714.
[8] Ceretti E, Giardini C, Attanasio A (2007) 3D Simulation and Validation of Tube Piercing Process. *Proceedings of the 9th International Conference on Numerical Methods in Industrial Forming Processes NUMIFORM07*, Porto, Portugal, 413–418.
[9] Lemaitre J, Desmorat R (2005) *Engineering Damage Mechanics*. Springer.
[10] Lemaitre J (1985) A Continuous Damage Mechanics Model for Ductile Fracture. *Journal of Engineering Materials and Technology* 107:83–88.